Electrically switchable phase-type fractal zone plates and fractal photon sieves

Yan Jun Liu,[1] Hai Tao Dai,[2] Xiao Wei Sun,[2,*] and Tony Jun Huang[1,*]

[1]*Department of Engineering Science and Mechanics, The Pennsylvania State University, University Park, Pennsylvania 16802, USA*

[2]*School of Electrical & Electronic Engineering, Nanyang Technological University, Nanyang Avenue, Singapore 639798, Singapore*

junhuang@psu.edu (T. J. H.); exwsun@ntu.edu.sg (X. W. S.)

Abstract: Electrically switchable phase-type fractal zone plates and fractal photon sieves were fabricated using polymer-dispersed liquid crystal material based on a photomask. While both exhibited similar first-order diffraction behavior, the fractal photon sieves showed greatly suppressed diffraction at higher orders. Compared with current amplitude-type photomasks, our switchable, phase-type devices demonstrated higher diffraction efficiency, an important factor in the future development of adaptive optics.

OCIS codes: (050.1970) Diffractive optics; (050.5080) Phase shift; (160.2100) Electro-optical materials; (230.3720) Liquid-crystal devices.

References and links

1. N. Bokor, and N. Davidson, "Ideal collimation, concentration, and imaging with curved diffractive optical elements," Rev. Sci. Instrum. **76**(11), 111101 (2005).
2. F. M. Dickey, "Laser beam shaping," Opt. Photonics News **14**, 30–35 (2003).
3. M. A. Forastiere, and G. C. Righini, "A new approach to the design of hybrid lenses for integrated optics," Opt. Rev. **6**(2), 124–130 (1999).
4. Y. X. Wang, W. B. Yun, and C. Jacobsen, "Achromatic Fresnel optics for wideband extreme-ultraviolet and X-ray imaging," Nature **424**(6944), 50–53 (2003).
5. G. Saavedra, W. D. Furlan, and J. A. Monsoriu, "Fractal zone plates," Opt. Lett. **28**(12), 971–973 (2003).
6. W. D. Furlan, G. Saavedra, and J. A. Monsoriu, "White-light imaging with fractal zone plates," Opt. Lett. **32**(15), 2109–2111 (2007).
7. J. A. Monsoriu, G. Saavedra, and W. D. Furlan, "Fractal zone plates with variable lacunarity," Opt. Express **12**(18), 4227–4234 (2004).
8. J. A. Davis, L. Ramirez, J. A. R. Martín-Romo, T. Alieva, and M. L. Calvo, "Focusing properties of fractal zone plates: experimental implementation with a liquid-crystal display," Opt. Lett. **29**(12), 1321–1323 (2004).
9. H. T. Dai, J. H. Liu, X. C. Sun, and D. J. Yin, "Programmable fractal zone plates (FraZPs) with foci finely tuned," Opt. Commun. **281**(22), 5515–5519 (2008).
10. L. Kipp, M. Skibowski, R. L. Johnson, R. Berndt, R. Adelung, S. Harm, and R. Seemann, "Sharper images by focusing soft X-rays with photon sieves," Nature **414**(6860), 184–188 (2001).
11. Q. Cao, and J. Jahns, "Focusing analysis of the pinhole photon sieve: individual far-field model," J. Opt. Soc. Am. A **19**(12), 2387–2393 (2002).
12. Q. Cao, and J. Jahns, "Nonparaxial model for the focusing of high-numerical-aperture photon sieves," J. Opt. Soc. Am. A **20**(6), 1005–1012 (2003).
13. G. Andersen, "Large optical photon sieve," Opt. Lett. **30**(22), 2976–2978 (2005).
14. R. Menon, D. Gil, G. Barbastathis, and H. Smith, "Photon-sieve lithography," J. Opt. Soc. Am. A **22**(2), 342–345 (2005).
15. G. Andersen, and D. Tullson, "Broadband antihole photon sieve telescope," Appl. Opt. **46**(18), 3706–3708 (2007).
16. J. Jia, J. Jiang, C. Xie, and M. Liu, "Photon sieve for reduction of the far-field diffraction spot size in the laser free-space communication system," Opt. Commun. **281**(17), 4536–4539 (2008).
17. F. Giménez, J. A. Monsoriu, W. D. Furlan, and A. Pons, "Fractal photon sieve," Opt. Express **14**(25), 11958–11963 (2006).
18. F. Gimenez, W. D. Furlan, and J. A. Monsoriu, "Lacunar fractal photon sieves," Opt. Commun. **277**(1), 1–4 (2007).
19. Y. J. Liu, X. W. Sun, P. Shum, and X. J. Yin, "Tunable fly's-eye lens made of patterned polymer-dispersed liquid crystal," Opt. Express **14**(12), 5634–5640 (2006).
20. Y. J. Liu, X. W. Sun, H. I. Elim, and W. Ji, "Gain narrowing and random lasing from dye-doped polymer-dispersed liquid crystals with nanoscale liquid crystal droplets," Appl. Phys. Lett. **89**(1), 011111 (2006).

#109954 - $15.00 USD Received 10 Apr 2009; revised 16 Jun 2009; accepted 24 Jun 2009; published 7 Jul 2009

21. Y. J. Liu, and X. W. Sun, "Electrically switchable computer-generated hologram recorded in polymer-dispersed liquid crystal," Appl. Phys. Lett. **90**(19), 191118 (2007).
22. Y. J. Liu, X. W. Sun, Q. Wang, and D. Luo, "Electrically switchable optical vortex generated by a computer-generated hologram recorded in polymer-dispersed liquid crystals," Opt. Express **15**(25), 16645–16650 (2007).
23. L. Zunino, and M. Garavaglia, "Fraunhofer diffraction by Cantor fractals with variable lacunarity," J. Mod. Opt. **50**(5), 717–727 (2003).
24. D. Wu, L.-G. Niu, Q.-D. Chen, R. Wang, and H.-B. Sun, "High efficiency multilevel phase-type fractal zone plates," Opt. Lett. **33**(24), 2913–2915 (2008).
25. H. Ren, Y.-H. Fan, and S.-T. Wu, "Tunable Fresnel lens using nanoscale polymer-dispersed liquid crystals," Appl. Phys. Lett. **83**(8), 1515–1517 (2003).

1. Introduction

Diffractive focusing elements play an important role in a wide range of applications, including light collimation [1], beam shaping [2], and aberration correction [3]. Among them, Fresnel zone plates (FZPs) do not require diffraction-limited, three-dimensional mirror surfaces, thus offering simple packaging and deployment [4]. Recently, Furlan *et al*. developed a new type focusing element: fractal zone plates (FraZPs) [5]. Similar to conventional FZPs, the FraZP produces multiple focal points along the optical axis when illuminated by plane waves. Each focal point shows a characteristic fractal structure, generating a self-similarity effect. Compared with FZPs, FraZPs can greatly enhance the imaging quality by increasing the depth of the field and reducing the chromatic aberrations [6]. In addition, by modifying the FraZP design [7–9], the focusing properties can be conveniently varied. For instance, Dai *et al*. demonstrated that the focal points of FraZPs can be finely tuned by changing the lacunarities, which could not be conveniently implemented by conventional FZPs [9].

Another type of diffractive optical elements, known as photon sieve [10], has been developed for focusing and imaging soft X-rays in high resolution. It is similar to a FZP, except that the clear zones in a FZP are replaced by a saturation of non-overlapping holes of set sizes in a photon sieve. Both theoretical and experimental works have been conducted on studying the fundamental properties of photon sieves [11,12] and demonstrating their practical applications [13–16]. Recently, by combining the concepts of the FraZP and the photon sieve, the fractal photon sieve (FraPS) [17,18] has been developed. It is anticipated that FraPS will not only have similar unique properties as FraZPs but also significantly suppress the high-order diffractions.

While the aforementioned amplitude-type optical elements have important applications based on their unique properties, each is limited by rather low diffraction efficiency (<1%) [13] and inability to be switched on/off or tuned once fabricated. In certain applications, continuous control of diffraction efficiency is necessary to eliminate the need for external amplitude spatial light modulators and to ease the adjustment for multiple optical wavelengths within an optical system. To address these two issues, electrically tunable phase-type focusing elements with high diffraction efficiency must be developed.

To this end, liquid crystal (LC)-based materials have been extensively explored for diffractive optics applications due to their electrically tunable properties. Among them, polymer-dispersed liquid crystal (PDLC) material stands out due to its versatile optical properties, simple fabrication, and fast response times. In our previous reports, different optical devices were demonstrated using PDLC materials, such as fly's-eye lenses [19], random lasers [20], information storages [21], and optical vortices [22]. These devices were all flat and electrically switchable, indicating that they could be conveniently integrated and adapted for various applications.

In this paper, we demonstrate electrically switchable phase-type FraZP and FraPS using PDLC material based on a photomask. Each device's focusing properties were examined and compared both theoretically and experimentally. Compared with amplitude-type FraZP and FraPS, these phase-type devices demonstrated higher diffraction efficiency (~6%). The improved diffraction efficiency and the electrically switchable capability presented here make the FraZP and FraPS one step closer in replacing the conventional FZPs in applications such as x-ray microscopy (where narrowband sources are hardly available), terahertz imaging and tomography, and ophthalmology.

#109954 - $15.00 USD Received 10 Apr 2009; revised 16 Jun 2009; accepted 24 Jun 2009; published 7 Jul 2009

2. Mask design

The fabrication process can be found elsewhere in more detail [5]. In brief, the first step was to define an initiator (stage S = 0). Next, at stage S = 1, the generator of the set was constructed by N non-overlapping copies of the initiator, each scaled by a factor $\gamma < 1$. At the following stages (S = 2, 3, ...), the generation process was repeated for each segment in the previous stage. In general, one has to use four parameters to characterize the FraZPs: fractal order, S, scaled factor, γ, the number of residual bars, N, and the lacunarity, ε. Using this rule, we generated a FraZP and FraPS with S = 2, N = 4, γ = 1/7, ε = 1/7, as shown in Fig. 1(a) and 1(b), respectively. Each had a 6.2 mm diameter and innermost zone width of ~1 mm. For the FraZP, the outermost zone width was ~40 μm. For the FraPS, the diameter, d, of the holes in each ring of width, w, had an optimum value to achieve effective focusing [10]. In our design, d/w was set to be 1.5. While the holes in the outermost zone of the FraPS were ~60 μm in diameter, the entire sieve consisted of 2627 holes of varying size. The ratio of the area covered by the holes to the total area of the corresponding zone was approximately 90%. Their diffraction patterns at the focal plane were simulated based on the Fresnel diffraction, as shown in Fig. 1(c) and 1(d). A sharp bright focus can be clearly seen in the center and the FraZP shows less scattering compared to the FraPS.

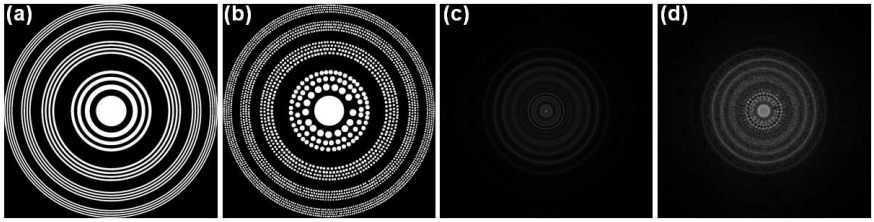

Fig. 1. Computer-generated (a) FraZP and (b) FraPS, and (c, d) their corresponding simulated diffraction patterns at the focal plane. The parameters used were S = 2, N = 4, γ = 1/7, and ε = 1/7.

3. Theory

When an optical system with two-dimensional pupil function $p(r, \phi)$ is illuminated by a plane wave with a wavelength of λ, the irradiance along the optical axis z can be expressed in canonical polar coordinates as expressed below:

$$\mathrm{I}(z)=\left(\frac{2\pi}{\lambda z}\right)^2\left|\int_0^a\int_0^{2\pi} p(r,\varphi)\exp\left(i\frac{\pi}{\lambda z}r^2\right)rdrd\varphi\right|^2. \qquad (1)$$

Based on the self-similar properties of the fractals and Fourier transforms, the irradiance along the optical axis of the FraZP can be expressed as follows [23]:

$$\mathrm{I}(z)=4^{2S+1}\sin^2\left(\pi\gamma^S\frac{a^2}{2\lambda z}\right)\left\{\prod_{i=1}^{S}\cos^2\left[\pi\frac{a^2}{2\lambda z}\gamma^i\left(\frac{1-\varepsilon}{\gamma}-2\right)\right]\cos^2\left[\pi\frac{a^2}{2\lambda z}\gamma^i\left(\frac{\varepsilon}{\gamma}+1\right)\right]\right\}. \qquad (2)$$

While for the FraPS, as pointed out in Ref [11], the axial irradiance it produces is insensitive to the angular distribution of the holes. Therefore, it can be approximately considered to be the superposition of the diffracted fields of every single hole, which is expressed as follows:

$$\mathrm{I}(z)=\sum_{n=1}^{N_h}\left|2N_f A_n\exp\left[jk\left(L_n+\frac{R'^2}{2z}\right)\right]Jinc\left(\frac{2\pi a_n}{\lambda z}\rho\right)\right|^2, \qquad (3)$$

where $N_f = \pi a_n^2/\lambda z$ is the Fresnel number, $A_n = A(x_n, y_n)$ is amplitude distribution, $L_n = L(x_n, y_n)$ is the eikonal, $Jinc(\cdot) = J_1(\cdot)/(\cdot)$, $J_n(\cdot)$ is the n^{th}-order Bessel function.

#109954 - $15.00 USD Received 10 Apr 2009; revised 16 Jun 2009; accepted 24 Jun 2009; published 7 Jul 2009

According to Eq. (2) and (3), the axial irradiance distribution of the FraZP and FraPS was calculated, respectively, as shown in Fig. 2(a) and 2(b). The FraZP and FraPS show similar focusing behaviors for the primary focus, the first-order diffraction. The size of the focal point, *i.e.*, full width at half maximum (FWHM), of a FraZP is determined by the width $w_{\min}$ of the outermost zone while the size of the focal point of a FraPS is determined by the ratio of the smallest hole size to the maximum d/w ratio, $d_{min}/(d/w)_{max}$ [10]. In our design, the FraZP and FraPS have the same FWHM (~40 μm) since we kept d/w unchanged. The main discrepancy between the FraZP and the FraPS is that the higher-order diffractions are greatly suppressed due to angular average effect for the FraPS.

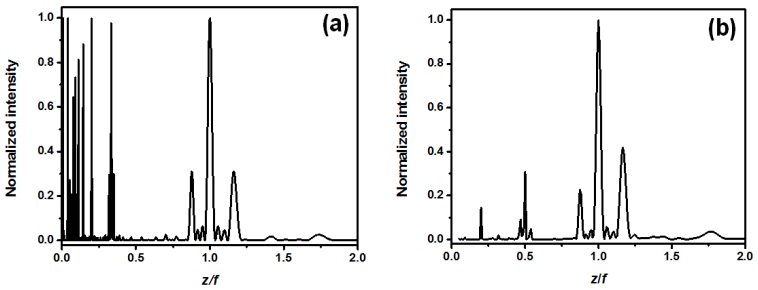

Fig. 2. Normalized irradiance distributions along the optical axis produced by a (a) FraZP and (b) FraPS, respectively.

4. Experiment

The LC/prepolymer syrup consisted of 48.09 wt% monomer, dipentaerythritol penta-/hexa-acrylate (DPPHA), 6.91 wt% cross-linking monomer, N-vinylpyrrollidone (NVP), 1.25 wt% photoinitiator, Rose Bengal (RB), 0.81 wt% coinitiator, N-phenylglycine (NPG), 9.84 wt% surfactant, oleic acid (OA), and 33.09 wt% LC E7. The LC E7 was purchased from Merck while the other materials were purchased from Sigma-Aldrich. The LC E7 had an ordinary refractive index of $n_o = 1.521$ and a birefringence of $\Delta n = 0.225$. Drops of the mixture were sandwiched between two pieces of indium-tin-oxide (ITO) coated glass to form a LC cell. The cell thickness was controlled to be ~10 μm by positioning plastic microbeads as spacers between the two pieces of ITO glass. A photomask was produced by transferring the computer-generated FraZP and FraPS patterns onto a transparency and then clipping them on the top of the LC cell. The LC cell was then subject to the exposure by a collimated laser beam (514.5 nm). During the recording process, the monomers polymerized first in the bright areas with high intensity. As a result, spatial gradients in chemical potential were established, which produced a diffusion of monomers (and other reactants) into the high-intensity regions, and a counter-diffusion of LCs into the low-intensity regions. Finally, patterns similar to the photomask were formed within the LC cell. The exposure intensity and time were 0.5 mW/cm^2 and 10 min, respectively.

Figure 3 depicts the experimental setup used to characterize the focusing properties of the FraZP and FraPS. The collimated He-Ne laser beam had a diameter of ~1 cm, which fully covered the entire effective area. A charge-coupled-device (CCD) camera (Imaging Solutions Group LW-1.3-S-1394-C) was used to study the focusing properties. By moving the CCD camera back and forth along the optical axis, the focal length can also be determined. Electro-optical measurements were carried out by applying a square waveform voltage with a frequency of 1 KHz on the sample using a voltage amplifier (Trek 677B-L-CE).

#109954 - $15.00 USD Received 10 Apr 2009; revised 16 Jun 2009; accepted 24 Jun 2009; published 7 Jul 2009

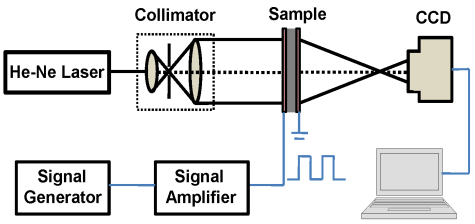

Fig. 3. The experimental setup to characterize the focusing properties of the FraZP and FraPS.

5. Results and discussion

The FraZP had a primary focal length of 38 cm and a secondary focal length of 30 cm, while the FraPS had a primary focal length of 37 cm and a secondary focal length of 31.5 cm. The measured primary FWHM of the FraZP and the FraPS were 80 μm and 56 μm, which were larger than the theoretical results (Section 3). A ~1 mm gap between the photomask and the recording material (an ITO glass substrate) was the main reason for the discrepancy between experimental and theoretical results. After a laser beam passed through the photomask, light diffracted while passing through the substrate. Based on single-slit diffraction approximation, this diffraction effect caused the light beam to diverge by an angle of $\sim\lambda/w_{min}$ for the FraZP and $\sim\lambda/d_{min}$ for the FraPS. Additionally, scattering and interference induced by the phase separation between the polymers and the LCs played another important role in the enlargement of the focal point. As a result, features recorded within the LC cell were larger than those on the photomask, thereby inducing a larger focal point. According to Fig. 2, the intensities of the primary and secondary focal points were almost the same in the FraZP, while in the FraPS, the intensity of the secondary focal point was greatly suppressed due to the angular average effect. We measured the intensities of the primary and secondary focal points of the FraZP and FraPS (Fig. 4) and found that they matched well with the theoretical results (Fig. 2). In the FraPS, the intensity for the secondary focal point (Fig. 4(h)) was suppressed to be almost half of the primary intensity (Fig. 4(g)).

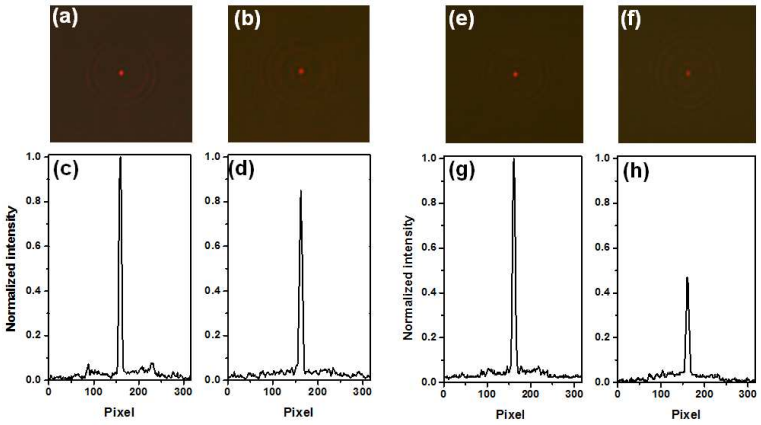

Fig. 4. CCD captured images of the (a) primary and (b) secondary focal points, and (c, d) their corresponding normalized intensity distribution for the FraZP. CCD captured images of the (e) primary and (f) secondary focal points, and (g, h) their corresponding normalized intensity distribution for the FraPS.

The first-order diffraction efficiency is determined by the relative phase difference between the adjacent zones. The relative phase difference $\Delta\delta$ can be written as

$$\Delta\delta = 2\pi(n_{even} - n_{odd})d/\lambda, \quad (4)$$

#109954 - $15.00 USD Received 10 Apr 2009; revised 16 Jun 2009; accepted 24 Jun 2009; published 7 Jul 2009

where d is the cell gap, λ is the wavelength, n_{even} and n_{odd} are the effective refractive index of even and odd zones, respectively. Being phase-type optical devices, the PDLC FraZP and FraPS are expected to produce higher efficiency than comparable amplitude-type devices. In our experiments, the measured diffraction efficiencies for the amplitude-type photomasks of the FraZP and FraPS were 0.92% and 0.73%, which are at the same level with the reported value, 0.35%, for an amplitude-type normal photon sieve [13]. The measured diffraction efficiencies of the PDLC FraZP and FraPS were 5.89% and 5.76%, which are much greater than the corresponding amplitude-type ones. We believe that with better phase separation between LCs and polymers, the efficiency can be further boosted as the theoretical value is 16.22% for a 2-level phase-type FraZP with $S = 2$, $N = 4$ [24].

For PDLC-based optical devices, a distinct advantage is that they can be electrically switched. Figure 5 shows the changes of the primary focus of the FraZP and FraPS under different applied voltages. The switching effect was clearly observed as the applied voltage increased. For both FraZP and FraPS, the intensity of the primary focus increased at first and then decreased as the electric field exceeded the threshold. This is because the phase difference between the even and odd zones changes with the applied electric field. A similar effect was observed by Ren *et al*. [25]. In our experiment, the threshold fields were ~2 V/μm for both the FraZP and FraPS, while the switching fields were 14 V/μm for the FraZP and 16 V/μm for the FraPS. After removing the electric field, the focal points returned to their initial states.

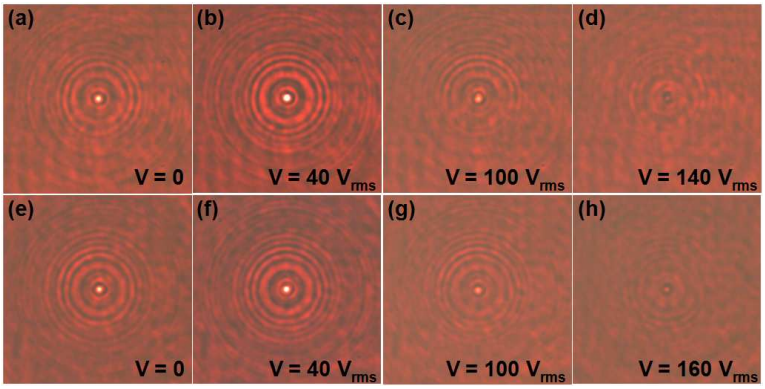

Fig. 5. Intensity changes of the primary focus for (a–d) FraZP (Media 1) and (e–h) FraPS (Media 2).

6. Conclusion

In summary, we have demonstrated electrically switchable phase-type FraZPs and FraPSs, and compared their focusing properties. While we observed similar first-order diffraction behavior in both FraZPs and FraPSs, higher-order diffraction in the FraPS was greatly suppressed. These phase-type optical devices demonstrated higher diffraction efficiency than those of amplitude-type counterparts. In addition, their electrically switchable capabilities make them useful as adaptive optical elements.

Acknowledgements

The authors thank Aitan Lawit for helpful discussion and manuscript preparation. This research was supported by the Air Force Office of Scientific Research (FA9550-08-1-0349), the National Science Foundation (ECCS-0801922 and ECCS-0609128), and the Penn State Center for Nanoscale Science (MRSEC). Components of this work were conducted at the Pennsylvania State University node of the NSF-funded National Nanotechnology Infrastructure Network.

#109954 - $15.00 USD Received 10 Apr 2009; revised 16 Jun 2009; accepted 24 Jun 2009; published 7 Jul 2009